A novel model of multicellular communication through extracellular matrix microstructure

John Metzcar[1,2], Ben S. Duggan[3,4], Brandon Fischer[1,5], Matthew Murphy[2,6] and Paul Macklin[1*]

[1]Intelligent Systems Engineering, Indiana University, 700 N. Woodlawn, Bloomington, 47408, Indiana, United States of America.

[2]Informatics, Indiana University, 901 E. Tenth Street, Bloomington, 47408, Indiana, United States of America.

[3]Computer Science, Indiana University, 700 N. Woodlawn, Bloomington, 47408, Indiana, United States of America.

[4]Current address - School of Medicine, Indiana University, Indianapolis, Indiana, United States of America.

[5]Current address - Abbott Diabetes Care, Oakland, California, United States of America.

[6]Current address - Humana, Cincinnati, Ohio, United States of America.

*Corresponding author(s). E-mail(s): macklinp@iu.edu;

Contributing authors: jpmetzca@iu.edu; bendugga@iu.edu; brandonfischer99@gmail.com; dmatthewmurphy@gmail.com;

Abstract

Extracellular matrix (ECM) is a key part of the cellular microenvironment and critical in multiple disease and developmental processes. Representing ECM and cell-ECM interactions is a challenging multi-scale problem that acts across the tissue and cell scales. While several computational frameworks exist for ECM modeling, they typically focus on

very detailed modeling of individual ECM fibers or represent only a single aspect of the ECM. Using the PhysiCell agent-based modeling platform, we combine aspects of previous modeling efforts and develop a framework of intermediate detail that addresses direct cell-ECM interactions. We represent a small region of ECM as an ECM element containing 3 variables: anisotropy, density, and orientation. We then place many ECM elements through a space to form an ECM. Cells have a mechanical response to the local ECM variables and remodel ECM based on their velocity. We demonstrate aspects of this framework with a model of cell invasion where the cell's motile phenotype is driven by the ECM microstructure patterned by prior cells' movements. Investigating the limit of high-speed communication and with stepwise introduction of the framework features, we generate a range of cellular dynamics and ECM patterns – from recapitulating a homeostatic tissue, to indirect communication of paths (stigmergy), to collective migration. When we relax the high-speed communication assumption, we find that the behaviors persist but can be lost as rate of signal generation declines. This result suggests that cell-cell communication mitigated via the ECM can constitute an important mechanism for pattern formation in dynamic cellular patterning while other processes likely also contribute to leader-follower behavior.

Keywords: extra-cellular matrix, agent-based modeling, collective migration, stigmergy

1 Introduction

Cell-cell communication drives many processes, from cell migration and growth to diseases such as breast cancer [1, 2]. This communication occurs through many mechanisms (e.g. contact, paracrine, or endocrine signaling). It also occurs through indirect cellular signaling mechanisms such as the alteration of the tissue microenvironment. Changing the extracellular matrix (ECM), the materials that holds tissues together, is one of the commonly deployed indirect cell communication mechanisms [1, 3–8]. Through its physical properties, such as fiber orientations, it provides cues for cellular migration and can serve as a conduit to inhibit or promote cell migration [1, 4, 9–11]. Carey et al. observed that fiber alignment induced anisotropic cell morphodynamics and spatial probing, guiding them along the axis of alignment while noting also that many questions remain unanswered regarding how cells navigate these environments [5]. In their review, Winkler et al. stated that remodeling of ECM can create paths leading cells out of ductal-carcinoma *in situ* [4]. Furthermore, signals from the ECM were implicated as influencing leader-follower migration, a form of collective cell movement where leader phenotype cells spearhead multicellular tissue invasion [12]. Multiple possible processes are shown to be at work in creating this leader-follower dynamic, with "action at a distance" via

writing signals to the matrix as one possible mechanism ready for investigation [1, 12]. Overall, dysregulation of ECM maintenance is associated with disease processes, in particular aspects of cancer progression and metastasis [4, 11, 13]

Given the importance of ECM in biological processes, there are multiple frameworks for modeling and simulation of ECM and cell-matrix interactions [14]. Broadly, they can be placed in four categories: discrete force-based, continuous force-based, single field, or other.

Examples of the discrete force-based frameworks include where both the migrating cells and individual matrix fibers are embodied as agents with direct forces dictating motility and realignment respectively [15]. Macnamara et al. also adopt this paradigm and couple with a model of blood vessel-cell interactions [16]. Other representations calculate forces over a network of individual spring-like elements. Zhu et al. construct ECM from a hook-and-spring network and Tozluoglu et al. model individual fiber filaments as hook-and-spring networks [17, 18].

continuous force-based models represent ECM as a continuously deformable material. Examples include van Oer et al., who use a finite element model of ECM coupled with a cellular-Potts model of cells and look at how stiffness and deformability of the ECM impact cell migration [19]. Ahmadzadeh et al. use a stress-strain relationship to deform fibers as well as incorporating cell adhesions to look at cellular level motility and morphology [20].

Single field (density) approaches to ECM often use partial-differential equations (PDEs) to update ECM density. Zeng et al. use a fibronectin "concentration" in developmental biology applications [21]. Daube et al. use a PDE for a scalar ECM density field in the context of sprouting angiogenesis in tumors [22]. Letort et al. use the PhyisBoSS framework (an implementation of PhyisCell [23] with the MaBoSS Boolean network simulator [24]) and also model ECM as a scalar-density field [25]. Trucu et al. model invasion as a moving value problem with ECM represented as a scalar field [26]. Building off of that work, Shuttleworth et al. 2019 and 2020 add non-local effects as well as orientation to the underlying moving boundary value of tumor invasion and adds matrix degradation respectively [27, 28].

Finally, there are other methods. Chauvier et al. and Hillen et al. use transport models to look at ECM [29, 30]. Other authors model ECM directly as a phase in an otherwise typical cellular-Potts model [31, 32]. Some authors also form long-range fibers by viewing sets of contiguous points occupied by ECM as fibers. This allows them to represent fiber orientation and length in addition to density [33, 34]. Finally Martinson et al. use a deposition of ECM puncta followed by cellular realignment of the fibers to study collective migration of neural crest cells using both number of ECM puncta and their orientations to alter cell motion [35].

In this work, we propose the approach of using a single phase of ECM with multiple variables (orientation, alignment, and density) modified via interactions with cells, which we represent as individual agents. This approach gives a simulation more expression than a density field. However, it does not require the detailed knowledge, assumptions, or simulations of ECM components of other frameworks while still generating insights into multi-cellular interactions.

To demonstrate the framework, we developed a model of cellular invasion. It is a two phenotype leader-follower model, inspired by the cancer biology literature [12, 36]. Leaders communicate their paths to follower cells by altering the ECM. The followers read the ECM cues and various collective behaviors result depending on simulation parameters. Using this model, in the limit of high communication potential, we observe stigmergy and collective invasion. Relaxing this assumption, we still see aspects of these behaviors but they diminish. This suggests that other mechanisms, such as strong cell-cell adhesion or chemical signaling, may also be present to produce the behaviors observed in the literature.

2 Methods

In this section, we first provide the conceptual background and mathematical formulation of the ECM and cell-ECM interactions framework (the ECM model). Then, we illustrate the framework with a series of computational experiments highlighting important aspects of the framework. Finally, we describe a model of cellular invasion used to explore our ECM model - a tumor spheroid simulation inspired by collective cell migration literature [12, 36].

2.1 ECM and cell-ECM interaction models

To enable explorations of ECM mitigated cellualar communication, we developed a three variable ECM representation and interaction rules for cells and the ECM. We use an agent-based approach to represent cells and a continuum model to represent the fine structure of ECM. Broadly, ECM elements are modified by cell movements and migration and in turn, cell motility is impacted by ECM components. Together, this constitutes a cell-cell communication method with the ECM modifications being the signal and changes in cell motility based on those changes the reading out of this signal.

2.1.1 Cell-based modeling framework

We use the PhysiCell tissue modeling system to impelement the ECM and cell-ECM interactions models [23]. PhysiCell uses a center-based, off-lattice representation of cells and implements physical cell-cell mechanics. It takes a phenotypic approach to encoding cell behaviors letting each cell-agent carry

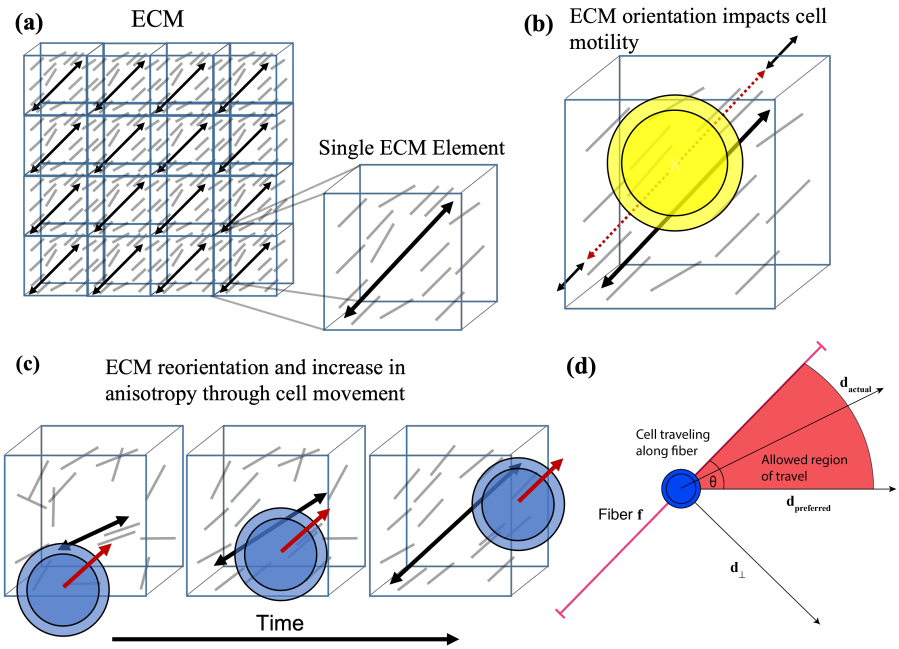

Fig. 1: **Schematic of ECM model and ECM based communication 1a** Illustrated here is an ECM, composed of tiled ECM elements. A single element contains many fibers (grey line segments) which we represent by an overall (average) fiber orientation and amount of self-alignment, or anisotropy (the black double-headed arrow and its length). **1b** An element's overall fiber orientation impacts a cell's motility, providing a preferred angle of travel through the element (dashed red arrow). The amount of influence is related to the amount of amount of anisotropy and the cell's ability to sense and respond to the ECM cues. **1c** Cell movement (cell direction - red arrow) remodels ECM by altering its elements' orientation and anisotropy. Cells align an element's orientation parallel to their direction of travel and increase anisotropy proportional to cell speed. **1d** Schematic for mathematical model of cell motility and fiber interactions. Cell shown in blue. See 8, 10, and 12 for variable explanations.

its own parameters and behavioral rules. To model the diffusive microenvironment, we use BioFVM, which comes with PhysiCell. BioFVM is a diffusion solver that uses a Cartesian representation of space and finite volume method to efficiently handle multiple diffusing substrates over tissue scale sized domains [37].

2.1.2 Extracellular representation

Our model is intended to capture key aspects of a small piece, or element, of ECM. We conceive of an element of ECM as having three variables: an average fiber orientation (*orientation*), a relative local fiber alignment correlation (*anisotropy*), and a quantity that captures the relative amount of material present in a element (*density*). Assembling many of these elements together makes a whole ECM. Figure 1a shows an ECM, which is comprised of tiled

ECM elements. The inset shows a single element. It is conceived of as containing many fibers (grey line segments). However, the individual fibers are unmodeled and instead fibers are represented as having an average orientation and anisotropy (the black double-headed arrow and its length) and volumetric density (illustrated as number of fibers per element in the schematic).

Mathematically, we center an element at a location $\mathbf{x}$ in space and define them as follows:

- ***Fiber orientation:*** $\mathbf{f}(\mathbf{x})$, the average local fiber direction, represented as a unit length 3 dimensional vector.
- ***Anisotropy:*** $a(\mathbf{x})$, average local fiber alignment correlation. At zero, there is no correlation and at one, locally there is complete fiber-to-fiber correlation.
- ***Fiber density:*** $\rho(\mathbf{x})$, volume fraction of fibers, which we will refer to as the average local fiber density. Zero refers to completely fluid filled and one to completely packed with fibers without void space.

Without a loss of generality, for our simulations and implementation, we arrange the units in a Cartesian grid.

2.1.3 Cell-ECM interactions: Model assumptions

We also model interactions between cells and the ECM. The conceptual model is below with more detailed information provided in Supplementary Material Sections 7.1 and 7.2.

ECM impacts cell migration:

- Fiber orientations provide directional cues.
- Anisotropy gives a strength of directional cue: high anisotropy increases an ECM element's influence on direction of cell migration.
- Density influences cell speed: too little ECM, cells have nothing to attach to; too much, cells cannot pass.

Cell migration and movement impact microstructure:

- Direction of cell migration reorients an ECM elements's fiber orientation.
- Cell-ECM element contact increases ECM anisotropy proportional to cell speed.
- Cells dynamically remodel ECM density towards a target value.

The interactions between the ECM and cells can be specified at the cellular level, allowing for a variety of cell-ECM interaction phenotypes. Our framework captures the range of biological behaviors: cells may be very sensitive to ECM cues or unable to read them, may be equipped with the machinery to remodel ECM or not [12]. Finally, we note and will demonstrate that these features can be integrated with others such as sensitivity to chemical cues and cell-cell adhesion and to obtain an even richer range of cell behaviors.

2.2 Individual features of the cell-ECM communication model

Results in this section isolate and demonstrate a single or small number of aspects of the cell-ECM interaction model presented in Section 2.1. To aid in isolating only ECM-to-cell and cell-to-ECM effects, in this section we disabled cell-cell mechanical interactions by setting both the adhesion and repulsion parameters of the standard PhysiCell model to zero [23]. We used multiple cells per result to highlight the uniformity of interactions across the computational domain and as a visual aid rather than to explore how the cell-cell interactions may impact the simulations.

Note that while the framework does include an ECM density and its updates and influence on cell behavior, it is not highlighted in our examples. However, we include the description, methods, and assumptions for this aspect of the model for the sake of completeness of the framework and leave it to future work and others to highlight.

2.2.1 Cells produce signals in the ECM

Combing the ECM: fiber orientation and alignment remodeling produces extended paths in the ECM

Remodeling of the ECM units can produce paths that ECM sensitive cells can then follow. In Figure 2a, cells move chemotactically with bias of 1 across a field of un-oriented ECM aligning it in the direction of travel. Each ECM element is initialized with a random orientation and uniformly with $a = 0.9$. Remodeling cells move across the domain, producing individual changes in ECM elements as they travel. After 4 passes of writing signals to the matrix, the ECM is aligned almost completely parallel to the direction of travel with most elements' anisotropy having increased to approximately 0.92, producing preferred paths of transit across the domain. A video is linked in the Supplemental Materials (Section 7.4.1) and available on YouTube Figure 2a - Cell March.

2.2.2 Cells read signals in the ECM, impacting their migration

All results in this section were produced with anisotropy and density uniformly set to 1.0 (maximum and most impactful value) and 0.5 (value of maximum cell speed) respectively and both the chemical and physical (ECM) environments not updating once initialized. This ensures that only dynamics between the cells and the ECM or respectively among the cells, ECM, and chemical field are isolated and other aspects held constant. Finally, the cells are highly sensitive to ECM ($s = 1.0$) as well as the chemical gradient ($b = 1.0$) when present.

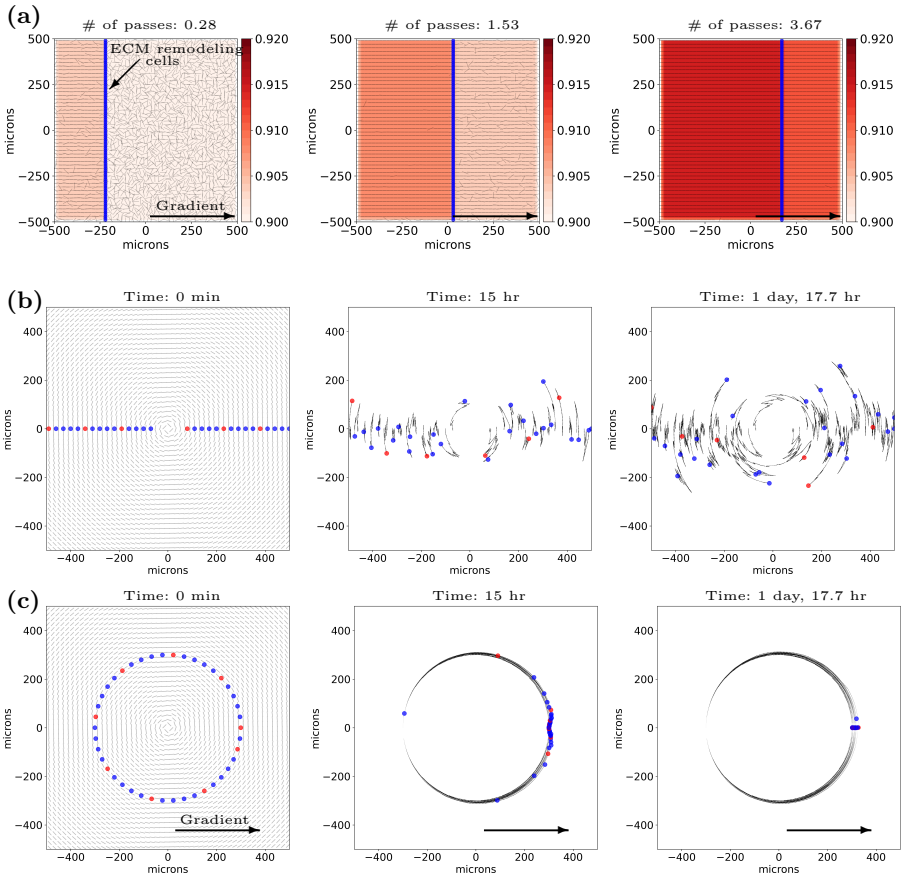

Fig. 2: **Highlights of individual aspects of the cell-ECM interactions:** Model results showing ECM remodeling cells altering ECM orientation and anisotropy (**2a**) A line of remodeling cells (blue circles), motivated by a constant chemical gradient (black arrow), move in the positive x-direction, reorienting an initially random field of orientations (black line segments) with uniform anisotropy of 0.90 (left-most image in **2a**). Upon reaching the simulation boundary, the cells are reset to the opposite edge, and remodeling continues (middle - 2 passes). At 4 passes, the ECM is almost completely reoriented parallel to the direction of travel of the cells and anisotropy has increased from 0.90 to ∼0.92 (left). Results of environmental reading are shown in **2b** and **2c**. Both simulations use an ECM that is highly anisotropic (a uniformly set to 1.0) and element orientations arranged to form approximate concentric circles. The simulation in **2b** begins with ECM reading cells almost equally spaced along the line x=0 (left most image - cells shown in red and blue; color is for visual contrast only). Cells follow the ECM circles closely in an approximate 1-D random walk, forming circular arcs (small black arrows marking cell position history every 6 minutes). As the rate of curvature of ECM cues decreases away from the center of the computational domain, the cells are better to follow the ECM circles. The simulation in **2c** contrasts with **2b** by providing an additional environmental cue - a chemical gradient. As the ECM sensitive cells integrate both signals, in contrast to **2b**, their motion is no longer random and they travel uniformly in the direction of the gradient. With a circular initial configuration (left), the cells follow each other along the same circle (middle and right), coming to a point of meta-stability where the ECM orientation is exactly perpendicular to the chemical field. As in **2b**, cells "jump" off the path set by the ECM by overshooting their original path prior to a cell motility update.

Cells can closely follow paths in the ECM

Supplementary Figure 1 shows influence of ECM on cell migration combined with a chemotactic field going to the right. The left-most subfigure shows the initial cell positions as well as the ECM element fiber orientations (45° and -45° from the x-axis in the top and bottom sections of the domain respectively). Without ECM influence, the cells would simply move to the right. Instead, the ECM biases the cell paths away from the path set by the gradient. The middle and right-most images include the cells positional history, shown as arrows trailing the blue and red cells (note in this and in all images in this section, the cell color is simply for visual contrast). A video is linked in the Supplemental Materials (Section 7.4.1) and available on YouTube Supplementary Figure 1 - Split ECM with chemotaxis.

Cells perform approximate 1-D random motion along ECM paths

Figure 2b shows the results of cell motion on circular ECM. We show the initial cell configuration as well as the ECM element orientations on the left with the middle and right images including cell positional history at 15 hours and 41.7 hours simulated time respectively. We observed cells having no apparent preferred direction (approximately 1-D random motion) along the ECM circles, as expected given the lack of bias along ECM orientations. Because of the curved tracks, contrasting with Supplementary Figure 1, cells move off their initial circles out to ECM circles of higher radius. Note also that cells placed or traveling further from the origin more closely follow the underlying ECM cues. The circles furthest from the origin produce the best approximations to true circles, while further into the domain, the error between a true circle and the discretized ECM increases. Due to the high error at the center of the domain, for this simulation, we exclude the central region with radius of 80 μm or less. A video is linked in the Supplemental Materials (Section 7.4.1) and available on YouTube Figure 2b - Circular ECM with no gradient.

Cells follow curved paths

Figure 2c shows the results of cell motion transitting circular ECM with an additional cue supplied by a chemical gradient. This additional information causes the cells to follow the ECM circle on which they were initially placed to the right (the direction of the chemical gradient). Note that at locations where the chemical gradient and ECM orientation are perpendicular, cells are in a quasi-stable state as the two directional cues cancel. This meta-stable state is seen in the lagging cell in the middle plot of Figure 2c. Note that all other cells in this plot, except the lagging blue cell on the left side of the image, have moved many cell lengths from their initial positions. This cell began at the x-axis, which defines a line in which all units of ECM have an orientation perpendicular to the chemical field. Likewise, all the cells converge at the x-axis, where their initial ECM contour becomes perpendicular to the chemical

field. Finally, as in Figure 2b, we observe mild "track jumping" as the cells do not converge to a single point, despite having all begun equidistant from the origin (on a shared circle of ECM). A video is linked in the Supplemental Materials (Section 7.4.1) and available on YouTube Figure 2c - Circular ECM with chemical gradient.

2.3 Cell invasion model

To explore our cell-ECM communication model in a rich setting and address questions centered on the mechanisms of tumor cell invasion, we developed a tissue simulation isolating invasive leader-follower behavior. It is inspired by the cancer biology literature [12, 36] and builds off of previous cell-based spheroid modeling work [23]. Mimicking [12], we include two cell phenotypes - leader cells endowed with more invasive behaviors (directed outward motility and ignorance to ECM cues) and follower cells with less invasive behaviors (random motility and response to ECM cues). Their observations suggest some form of communication between the leaders and followers; we model that communication through signals carried in and read from ECM using our cell-ECM interaction model with leaders producing signals and followers reading them. Simulating these phenotypes with our cell-ECM interaction model lets us explore and test for the microenvironmental conditions and behaviors required for collective migration. The simulation was implemented in PhysiCell 1.4.1 as a 2-D simulation (single slice of a 3-D environment). Brief details on each component of these simulations follow.

Table 1: **Cell-based model:** principle behaviors, parameters, and systems effects

Phenotype	Behavior	Key parameter(s)	Key outputs
Leader cells	ECM remodeling	Cellular rate of matrix realignment, rate of anisotropy growth	Lays cues for followers to sense
	Chemotaxis	Bias	Enables production of coherent paths
	Cell-cell adhesion and repulsion	Ratio of adhesion strength to repulsion strength	Enables collective cell migration
Follower cells	ECM sensing	Cell ECM sensitivity	Allows cells to use cues in the ECM
	Chemotaxis	Bias	Enables coherent migration
	Cell-cell adhesion and repulsion	Ratio of adhesion strength to repulsion strength	Enables collective cell migration
	Random motion	Cell ECM sensitivity	Enables finding of paths in the ECM

2.3.1 Cellular modeling

We model two different phenotypes - leader cells and follower cells. These cells represent invasive and non-invasive cancer cells, respectively. The key rules of the cell invasion/leader follower model are summarized in Table 1. In particular, leader cells follow oxygen gradients with a high chemotactic bias ($b_l = 0.95$) (Equation 15) and encode their movements via ECM remodeling (see Section 7.1 for details). Followers movements are heavily influenced by signals in the ECM while also being mildly sensitive to chemotactic cues ($b_f = 0.05$) when in anisotropic ECM (Equation 16 - see Section (7.2 for mathematical details). They read signals in the ECM with a high sensitivity ($s = 1.0$) and are incapable of remodeling ECM. Thus, in highly anisotropic ECM, followers follow ECM dictated paths up the chemical gradient while in unaligned ECM, they move randomly. For implementation, we used the default cell phenotype from PhysiCell. To ensure that the physical interactions among the cells and their environment are driving dynamics, we do not allow cell proliferation or death. In general, unless otherwise noted, the cells were initialized with the default values and functions from PhysiCell. See the Supplemental Material Table 2 for additional parameter values.

2.3.2 Tissue microenvironment

We employ the native reaction-diffusion-decay simulator in Physicell, BioFVM, [37] to simulate the chemical microenvironment. We simulate avascular tissue with a diffusing oxygen-like field coming from the domain boundaries (Dirichlet conditions). Cells uptake oxygen and there is decay in the cellular milieu. Unless otherwise specified, we use default values from PhysiCell/BioFVM. These values give a diffusion length scale of 100 μm for regions of high cell density. We pre-condition the domain by running the diffusion solver for 10 simulated minutes before starting cellular simulation. See Supplemental Material Table 3 for additional details.

For ECM, we use the model described in Section 2.1. We place the ECM elements overlaying the BioFVM chemical environment (voxels) exactly unless otherwise noted. The two meshes explicitly have a shared origin and coordinate system. The ECM is initialized uniformly as completely isotropic, of ideal density for cellular motion ($\rho = 0.5$), and with random fiber orientations. See Supplemental Material Table 4 for additional details.

2.3.3 Tissue

Cells are placed at the center of the computational domain in a circular region of radius 175 μm and randomly assigned to be either followers or leaders. Cells are initialized at equilibrium spacing with six neighbors (hexagonal packing). See the Supplemental Material Table 5 for additional details.

2.4 Computational method details

This work implemented and run in PhysiCell 1.4.1 [23]. All codes are available with a permissive BSD license, including the ECM extensions, at GitHub. The release for this paper is located here. A free, interactive cloud-hosted version of the cell invasion model, using the ECM and cell-ECM frameworks, is available at nanoHUB.

We performed model exploration using DAPT 0.9.2. DAPT is a straightforward way to organize model exploration on a mixed compute resources for small teams. For more information see [38].

We used xml2jupyter to transform this command line C++ code into a cloud-hosted model with a GUI that can run without the need to download and compile the code [39]. This version is the version available at nanoHUB.

3 Results of cell invasion simulations and ECM mitigated communication model

Using our cell invasion model, we look at both a limit case and more general ECM remodeling paradigm. We start with the limit case of instant signal writing (instant ECM remodeling) and then present results of the finite signal generation.

3.1 Signal generation and reading are required for collective behavior

Isolating two model rules, the ability to produce and read signals, while also allowing cell-cell repulsion, we see that both environmental modification (signal generation) and ECM sensitivity (environmental reading) are required for collective migration. In Figure 3, we observe similar behavior of leaders and followers with ECM writing only (left column) and ECM reading only (middle column) simulations. Leaders separate from the initial disc of cells and reach the simulation boundary around 16 hours while followers remain roughly in the center of the domain. Only with both writing and reading (right column), are most cells able to escape the domain center and invade their surroundings. Here, we observe stigmergy, a form of collective behavior produced by indirect communication where signals encoded by agents enable other agents to follow the first agents' paths.

3.2 Adding cell-cell adhesion is required to enable collective migration

Adding cell-cell adhesion, we find a range of tissue morphologies, including collective migration. With mechanical interactions on and varying cell speed,

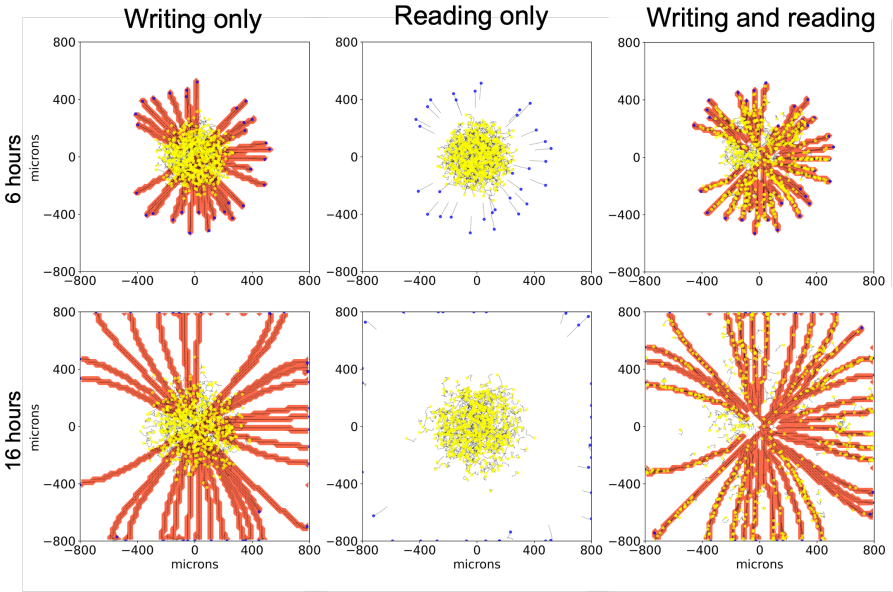

Fig. 3: **Communication of cell path through environmental modification produces invasive, stigmergic cell behavior:** Modification of the environment (left) and reading of the environmental signals (middle) separately do not produce collective behavior. With both together (right column) we observe that most cells escape the domain center and invade their surroundings via stigmergy. Initial configuration - 703 agents (5 % leaders) in 175 μm circle. Yellow agents: followers. Blue agents: leaders. Red contour plot: ECM anisotropy - uniformly equal to one in remodeled ECM elements. Line segments: ECM orientation. Black arrows: cell positional history, going back 12 samples (sampled every 6 minutes).

we see that ECM mediated communication can still produce stigmergy (Figure 4a). Additionally, in Figure 4b, we see that leaders have migrated to the leading edge of a clumps of mostly follower cells. Cells generally stay in contact with each other, producing a leader-follower collective migration. Finally, when cell speed is low, adhesion takes over cell mechanics and tissue morphology is constant over the computational experiment (Figure 4c). These results show that direct cell-cell communication through cell-cell adhesion and signals in the ECM microstructure are required for collective migration.

3.3 Collective migration is retained in the context of noisy communication

Having shown that the cell-ECM model is capable of producing a range of behaviors in the limit of high communication speed, we relax this limit assumption. Figure 5 contrasts the results of the limit of instant signal writing versus finite signal writing. Figure 5a shows two time points using the limit model, with cell speed of 0.5 μm/min and adhesion value of 10 μm/min. As in Figure 4, cell speed and adhesion are relatively balanced. In the earlier time point (top), we see what was the initial cluster of cells with one smaller cluster broken off

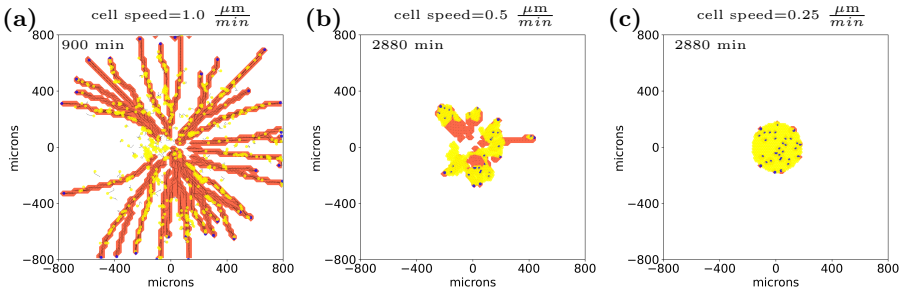

Fig. 4: **Multiple behaviors are captured with cell-ECM model:** With cell-cell adhesion on (adhesion = 10 $\frac{\mu m}{min}$), multiple behavioral regimes are observed within the limit of high writing potential. In **(a)** we see stigmergy with followers (yellow cells) following trails left by leaders (blue cells), as in Figure 3. Decreasing the cell speed by half to 0.5 $\frac{\mu m}{min}$ yields collective migration **(b)**. In **(c)** with cell speed again halved (s=0.25 $\frac{\mu m}{min}$), cell-cell adhesion cannot be overcome and the tissue morphology is frozen in the initial configuration. Initial configuration - 703 agents (5 % leaders) in 175 μm circle. Adhesion set to 10 $\frac{\mu m}{min}$. Yellow agents: followers. Blue agents: leaders. Red contour plot: ECM anisotropy - uniformly equal to one in remodeled ECM elements. Line segments: ECM orientation. Black arrows: cell positional history, going back 12 samples (sampled every 6 minutes).

with others soon to follow. In the next time point, we see that mostly mixed clusters remain, many having traveled well beyond their initial positions. This is a direct leader-follower migration. In Figure 5b, relaxing instantaneous signal writing, we observe that collective migration still occurs. Leaders remain in contact with followers and lead them out of the center of the domain. As the signals to followers are not as uniform or strong, the leaders break away and do not stay in contact as long as in the limit simulations. Because of delays in remodeling the environment as well as multiple interactions impacting that remodeling (cell-cell mechanics and local oxygen gradients), the ECM based communication signals are relatively noisy and lacking in strength. Instantaneous remodeling lets us remove those influences producing a much less noisy signal. However, strong enough paths are generated to enable followers to continue out behind the leaders via stigmergic behavior. Furthermore, overall migration appears to actually be enhanced with leaders pulling out cells behind them before finally breaking away. See for Supplementary Section 7.4.2 for links to videos.

Collective migration behavior in the finite signal writing scenario is sensitive to remodeling parameters and is lost with a less than order of magnitude change in them as seen in Supplementary Figure 2. Fiber reorientation and realignment rates vary by a factor of 4 in the two simulations. Another interesting observation is that it is possible to recover some aspects of collective migration by increasing the communication length scale, as shown in Supplementary Figure 3. Increasing the communication length scale effectively lets cells produce and read signal over a larger area, as if they are sensing/influencing a region much larger than their diameter. In terms of signal production, this is similar to having a higher rate of realignment as the leaders are in contact with a signal element of ECM for a longer time.

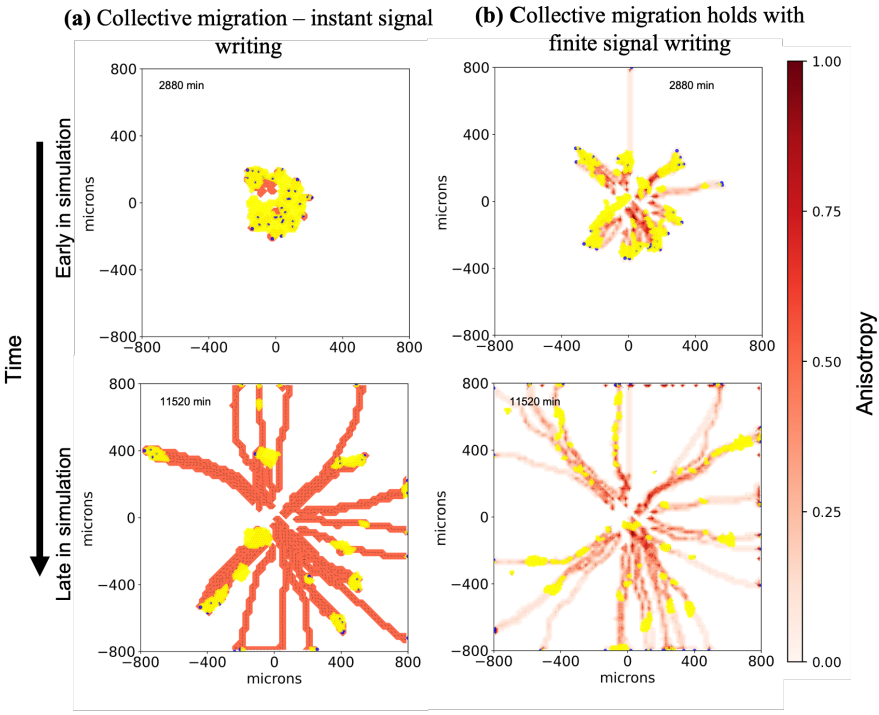

Fig. 5: **Collective migration is retained in the context of noisy communication** In the limit of instant signal generation, we see collective migration with mixed clumps of both leader (blue) and follower (yellow) cells migrating together (**(5a)** and Fig 4**b**). As seen in (**5b**), this behavior is robust to non-instant signal writing (ie - modification of ECM variables). Here, leaders stay in contact with followers and lead them out of the center of the domain. They do not stay in contact as long as in **(5a)** but strong enough paths are generated to enable followers to continue out via stigmergy. This behavior is sensitive to remodeling parameters and is lost with a less than order of magnitude change in them. See Supplementary Material Figure 2. Fiber realignment rate: 0.004 min^{-1}, fiber reorientation rate: 4 min^{-1}. Initial configuration - 703 agents (5 % leaders) in 175 μm circle. Adhesion set to 10 $\frac{\mu m}{min}$. Yellow agents: followers. Blue agents: leaders. Contour plots: ECM anisotropy - (**(5a)**) uniformly equal to one in remodeled ECM elements and (**(5b)** color bar. Line segments: ECM orientation. Black arrows: cell positional history, going back 12 samples (sampled every 6 minutes).

4 Discussion

In this work, we presented a novel mathematical and computational framework of multicellular communication mediated through ECM microstructure. As cells move, they modify the ECM and change behaviors in response to cues generated by those modifications, enabling communication of their paths. The framework captures multiple aspects ECM (orientation, strength of fiber-fiber self-alignment, and density) in a single field - an array of ECM elements. This adds to available methods for computational investigation of ECM dynamics and cell-ECM interactions. After showing model behavior for individual agents, we investigated a cellular invasion model inspired by the observations of leader-follower behavior in breast cancer [12]. We explored the leader-follower model

by looking at the limit of high fidelity communication, using an instantaneous rate of writing signals through ECM modification. Through iterative addition of interactions, we showed that the invasive cell model required ECM mediated communication to produce collective behavior (stigmergy) and furthermore required cell-cell adhesion to enable collective invasion. We observed that the collective behavior was sensitive to noise and signal strength with collective invasion possible for a range of remodeling rates but not guaranteed.

Figure 2 and accompanying videos (see Supplemental Material Section 7.4.1) demonstrate features of our cell-ECM interaction model and show the correspondence between expected and actual behaviors of the model. The ECM is remodelable by cell agents (Figure 2a) and can influence cell migration. Supplementary Figure 1 and Figure 2b and c highlight important aspects of how agent motility and environmental cues interact. Figure 2b shows that cells may miss ECM cues, especially in regions of high curvature. If cell agents completely traverse an ECM element prior to a motility update and the next cue they read is greatly out of line with the previous cue, the cells will miss the path. This shows that in our model, paths of high curvature (with respect to the cell persistence time and speed) may be missed. Figure 2c demonstrates another interesting aspect of our cell-ECM framework. If a cell receives two mutually perpendicular cues that it is equally influenced by that cell can become stuck. This is an extreme condition as in a typical simulation, we would not expect that an agent could achieve a perfect alignment of an ECM element and a conflicting cue. Without a perfect alignment, the agent will slow at that location, but will not stop. Overall, these results also show that in our model, on highly anisotropic ECM, ECM sensitive cells can perform approximate 1-D random motion (Figure 2b) while when given an additional cue, unidirectional motility appears (Figure 2d and Supplementary Figure 1).

With the strong signals laid by instant remodeling of the ECM, we observed two kinds of collective behavior realized via ECM-based communication - stigmergy and collective migration in Figures 3 and 4. These behaviors, in particular collective migration, were also observed when the communication rate was reduced to finite time scales (Figure 5b). Unexpectedly, overall escape and invasion appears to be enhanced with slower signal writing, perhaps due to the cells' greater ability to move more independently. However, as rates of signal generation continue to decrease (within one order of magnitude from the rates in (Figure 5b), forms of collective behavior were no longer observed (Supplementary Figure 2). This suggests that in the cases where communication is slow compared to cell speeds, some other mechanism must compensate when collective behaviors are observed, such as the leader-follower migration seen in [12]. To that end, we also explored increasing the communication length scale and find that collective migration was recovered, but not stigmergy (Supplementary Figure 3).

We observed that we needed to give the follower cells an additional bias beyond cell-cell contact to allow them to move as one along the cues written in the

ECM. In our model, we use oxygen chemotaxis in the follower cell population. In reality, it could also be a chemotactic cue coming from the leaders, some matrix factor the leaders release, or some other signal that leads them [4, 12].

Also, our current cell modeling framework does not allow for asymmetric rates of cell-cell attachment nor asymmetric adhesion such that a follower might could have a different adhesion strength to a follower versus a leader phenotype cell. Introducing spring-like attachments with different rates of attachment versus detachment adhesion would better mimic actual cell adhesion [40]. This enhanced adhesion might facilitate the ability of ECM signals to enable collective migration, even in the absence of an additional directional cue such as an oxygen gradient.

We note that our model of ECM captures only local remodeling. This contrasts with other models' ability to capture the network like connections within a full ECM (eg - [17]). To produce a computationally efficient ECM, we accept this limit. In the future, we may explore spreading remodeling over multiple ECM elements, for example with Gaussian smoothing.

5 Funding

We thank the Jayne Koskinas Ted Giovanis Foundation for Health and Policy for generous support. Additionally, this work was partially supported by the National Science Foundation (Grants 1735095 and 1720625).

6 Acknowledgements

We would like to thank Michael Getz, Randy Heiland, and Adrianne Jenner for their expertise and assistance with this work. We gratefully acknowledge access to FutureSystems at the Digital Science Center, Luddy School of Informatics, Computing, and Engineering.

References

[1] Cheung, K.J., Ewald, A.J.: Illuminating breast cancer invasion: Diverse roles for cell–cell interactions. Current Opinion in Cell Biology **30**, 99–111 (2014). https://doi.org/10.1016/j.ceb.2014.07.003

[2] Hanahan, D., Weinberg, R.A.: Hallmarks of Cancer: The Next Generation. Cell **144**(5), 646–674 (2011). https://doi.org/10.1016/j.cell.2011.02.013

[3] Humphrey, J.D., Dufresne, E.R., Schwartz, M.A.: Mechanotransduction and extracellular matrix homeostasis. Nature Reviews Molecular Cell Biology **15**(12), 802–812 (2014). https://doi.org/10.1038/nrm3896

[4] Winkler, J., Abisoye-Ogunniyan, A., Metcalf, K.J., Werb, Z.: Concepts of extracellular matrix remodelling in tumour progression and metastasis. Nature Communications **11**(1), 5120 (2020). https://doi.org/10.1038/s41467-020-18794-x

[5] Carey, S.P., Goldblatt, Z.E., Martin, K.E., Romero, B., Williams, R.M., Reinhart-King, C.A.: Local extracellular matrix alignment directs cellular protrusion dynamics and migration through Rac1 and FAK. Integrative Biology **8**(8), 821–835 (2016). https://doi.org/10.1039/C6IB00030D

[6] Frantz, C., Stewart, K.M., Weaver, V.M.: The extracellular matrix at a glance. Journal of Cell Science **123**(24), 4195–4200 (2010). https://doi.org/10.1242/jcs.023820

[7] LeBleu, V.S., MacDonald, B., Kalluri, R.: Structure and Function of Basement Membranes. Experimental Biology and Medicine **232**(9), 1121–1129 (2007). https://doi.org/10.3181/0703-MR-72

[8] Macklin, P., Edgerton, M.E., Thompson, A.M., Cristini, V.: Patient-calibrated agent-based modelling of ductal carcinoma in situ (DCIS): From microscopic measurements to macroscopic predictions of clinical progression. Journal of Theoretical Biology **301**, 122–140 (2012). https://doi.org/10.1016/j.jtbi.2012.02.002

[9] Werb, Z., Sympson, C.J., Alexander, C.M., Thomasset, N., Lund, L.R., MacAuley, A., Ashkenas, J., Bissell, M.J.: Extracellular matrix remodeling and the regulation of epithelial-stromal interactions during differentiation and involution. Kidney international. Supplement **54**, 68–74 (1996)

[10] Ewald, A.J., Brenot, A., Duong, M., Chan, B.S., Werb, Z.: Collective Epithelial Migration and Cell Rearrangements Drive Mammary Branching Morphogenesis. Developmental Cell **14**(4), 570–581 (2008). https://doi.org/10.1016/j.devcel.2008.03.003

[11] Lu, P., Takai, K., Weaver, V.M., Werb, Z.: Extracellular Matrix Degradation and Remodeling in Development and Disease. Cold Spring Harbor Perspectives in Biology **3**(12), 005058–005058 (2011). https://doi.org/10.1101/cshperspect.a005058

[12] Cheung, K.J., Gabrielson, E., Werb, Z., Ewald, A.J.: Collective Invasion in Breast Cancer Requires a Conserved Basal Epithelial Program. Cell **155**(7), 1639–1651 (2013). https://doi.org/10.1016/j.cell.2013.11.029

[13] Nguyen-Ngoc, K.-V., Cheung, K.J., Brenot, A., Shamir, E.R., Gray, R.S., Hines, W.C., Yaswen, P., Werb, Z., Ewald, A.J.: ECM microenvironment regulates collective migration and local dissemination in normal and

malignant mammary epithelium. Proceedings of the National Academy of Sciences **109**(39), 2595–2604 (2012). https://doi.org/10.1073/pnas.1212834109

[14] Metzcar, J., Wang, Y., Heiland, R., Macklin, P.: A Review of Cell-Based Computational Modeling in Cancer Biology. JCO Clinical Cancer Informatics (3), 1–13 (2019). https://doi.org/10.1200/CCI.18.00069

[15] Schlüter, D.K., Ramis-Conde, I., Chaplain, M.A.J.: Computational Modeling of Single-Cell Migration: The Leading Role of Extracellular Matrix Fibers. Biophysical Journal **103**(6), 1141–1151 (2012). https://doi.org/10.1016/j.bpj.2012.07.048

[16] Macnamara, C.K., Caiazzo, A., Ramis-Conde, I., Chaplain, M.A.J.: Computational modelling and simulation of cancer growth and migration within a 3D heterogeneous tissue: The effects of fibre and vascular structure. Journal of Computational Science **40**, 101067 (2020). https://doi.org/10.1016/j.jocs.2019.101067

[17] Zhu, J., Mogilner, A.: Comparison of cell migration mechanical strategies in three-dimensional matrices: A computational study. Interface focus **6**(5), 20160040 (2016). https://doi.org/10.1098/rsfs.2016.0040

[18] Tozluoğlu, M., Tournier, A.L., Jenkins, R.P., Hooper, S., Bates, P.A., Sahai, E.: Matrix geometry determines optimal cancer cell migration strategy and modulates response to interventions. Nature Cell Biology **15**(7), 751–762 (2013). https://doi.org/10.1038/ncb2775

[19] van Oers, R.F.M., Rens, E.G., LaValley, D.J., Reinhart-King, C.A., Merks, R.M.H.: Mechanical Cell-Matrix Feedback Explains Pairwise and Collective Endothelial Cell Behavior In Vitro. PLOS Computational Biology **10**(8), 1003774 (2014). https://doi.org/10.1371/journal.pcbi.1003774

[20] Ahmadzadeh, H., Webster, M.R., Behera, R., Jimenez Valencia, A.M., Wirtz, D., Weeraratna, A.T., Shenoy, V.B.: Modeling the two-way feedback between contractility and matrix realignment reveals a nonlinear mode of cancer cell invasion. Proceedings of the National Academy of Sciences **114**(9), 1617–1626 (2017). https://doi.org/10.1073/pnas.1617037114

[21] Zeng, W., Thomas, G.L., Glazier, J.A.: Non-Turing stripes and spots: A novel mechanism for biological cell clustering. Physica A: Statistical Mechanics and its Applications **341**, 482–494 (2004). https://doi.org/10.1016/j.physa.2004.03.089

[22] Daub, J.T., Merks, R.M.H.: A Cell-Based Model of Extracellular-Matrix-Guided Endothelial Cell Migration During Angiogenesis. Bulletin of

Mathematical Biology **75**(8), 1377–1399 (2013). https://doi.org/10.1007/s11538-013-9826-5

[23] Ghaffarizadeh, A., Heiland, R., Friedman, S.H., Mumenthaler, S.M., Macklin, P.: PhysiCell: An open source physics-based cell simulator for 3-D multicellular systems. PLOS Computational Biology **14**(2), 1005991 (2018). https://doi.org/10.1371/journal.pcbi.1005991

[24] Stoll, G., Caron, B., Viara, E., Dugourd, A., Zinovyev, A., Naldi, A., Kroemer, G., Barillot, E., Calzone, L.: MaBoSS 2.0: An environment for stochastic Boolean modeling. Bioinformatics **33**(14), 2226–2228 (2017). https://doi.org/10.1093/bioinformatics/btx123

[25] Letort, G., Montagud, A., Stoll, G., Heiland, R., Barillot, E., Macklin, P., Zinovyev, A., Calzone, L.: PhysiBoSS: A multi-scale agent-based modelling framework integrating physical dimension and cell signalling. Bioinformatics **35**(7), 1188–1196 (2019). https://doi.org/10.1093/bioinformatics/bty766

[26] Trucu, D., Lin, P., Chaplain, M.A.J., Wang, Y.: A Multiscale Moving Boundary Model Arising in Cancer Invasion. Multiscale Modeling & Simulation **11**(1), 309–335 (2013). https://doi.org/10.1137/110839011

[27] Shuttleworth, R., Trucu, D.: Multiscale Modelling of Fibres Dynamics and Cell Adhesion within Moving Boundary Cancer Invasion. Bulletin of Mathematical Biology **81**(7), 2176–2219 (2019). https://doi.org/10.1007/s11538-019-00598-w

[28] Shuttleworth, R., Trucu, D.: Cell-Scale Degradation of Peritumoural Extracellular Matrix Fibre Network and Its Role Within Tissue-Scale Cancer Invasion. Bulletin of Mathematical Biology **82**(6), 65 (2020). https://doi.org/10.1007/s11538-020-00732-z

[29] Chauviere, A., Hillen, T., Preziosi, L.: Modeling cell movement in anisotropic and heterogeneous network tissues. Networks & Heterogeneous Media **2**(2), 333–357 (2007). https://doi.org/10.3934/nhm.2007.2.333

[30] Hillen, T.: M5 mesoscopic and macroscopic models for mesenchymal motion. Journal of Mathematical Biology **53**(4), 585–616 (2006). https://doi.org/10.1007/s00285-006-0017-y

[31] Rubenstein, B.M., Kaufman, L.J.: The Role of Extracellular Matrix in Glioma Invasion: A Cellular Potts Model Approach. Biophysical Journal **95**, 5661–5680 (2008). https://doi.org/10.1529/biophysj.108.140624

[32] Scianna, M., Preziosi, L., Wolf, K.: A Cellular Potts model simulating cell

migration on and in matrix environments. Mathematical Biosciences and Engineering **10**(1), 235–261 (2013). https://doi.org/10.3934/mbe.2013.10.235

[33] Szabó, A., Varga, K., Garay, T., Hegedűs, B., Czirók, A.: Invasion from a cell aggregate—the roles of active cell motion and mechanical equilibrium. Physical Biology **9**(1), 016010 (2012). https://doi.org/10.1088/1478-3975/9/1/016010

[34] Kumar, S., Kapoor, A., Desai, S., Inamdar, M.M., Sen, S.: Proteolytic and non-proteolytic regulation of collective cell invasion: Tuning by ECM density and organization. Scientific Reports **6**(1), 19905 (2016). https://doi.org/10.1038/srep19905

[35] Martinson, W.D., McLennan, R., Teddy, J.M., McKinney, M.C., Davidson, L.A., Baker, R.E., Byrne, H.M., Kulesa, P.M., Maini, P.K.: Dynamic Fibronectin Assembly and Remodeling by Leader Neural Crest Cells Prevents Jamming in Collective Cell Migration. arXiv (2022). https://doi.org/10.48550/arXiv.2209.07794

[36] Carey, S.P., Starchenko, A., McGregor, A.L., Reinhart-King, C.A.: Leading malignant cells initiate collective epithelial cell invasion in a three-dimensional heterotypic tumor spheroid model. Clinical & Experimental Metastasis **30**(5), 615–630 (2013). https://doi.org/10.1007/s10585-013-9565-x

[37] Ghaffarizadeh, A., Friedman, S.H., Macklin, P.: BioFVM: An efficient, parallelized diffusive transport solver for 3-D biological simulations. Bioinformatics **32**(8), 1256–1258 (2016). https://doi.org/10.1093/bioinformatics/btv730

[38] Duggan, B., Metzcar, J., Macklin, P.: DAPT: A package enabling distributed automated parameter testing. Gigabyte **2021**, 1–10 (2021). https://doi.org/10.46471/gigabyte.22

[39] Heiland, R., Mishler, D., Zhang, T., Bower, E., Macklin, P.: Xml2jupyter: Mapping parameters between XML and Jupyter widgets. Journal of Open Source Software **4**(39), 1408 (2019). https://doi.org/10.21105/joss.01408

[40] Ozik, J., Collier, N., Heiland, R., An, G., Macklin, P.: Learning-accelerated Discovery of Immune-Tumour Interactions. Preprint, Systems Biology (March 2019). https://doi.org/10.1101/573972

7 Supplementary Material

7.1 Cell remodeling of ECM: Signal writing

Here we detail the mathematical models for updating ECM density, anisotropy, and orientation - the methods of writing a signal to the matrix. The ECM elements and cells are conceived of as being in close contact; cells alter the ECM element they are physically in. To formalize which ECM element a cell modifies out of the many possible options (see Figure 1a), we define cells as interacting with whichever element their center coordinates are the closest to, as in [23]. To do this, suppose cell i is at position $\mathbf{x_i}$. We remodel the ECM element whose center is closest to $\mathbf{x_i}$. We outline two related methods for writing signals - the limit case of instantaneous signal writing and the non-instantaneous case.

Limit of high writing potential

To explore an extreme case of ECM mediated communication, we model anisotropy and ECM element orientation as being immediately remodeled when contacted by a remodeling cell, resulting in the following relationships to update a and $\mathbf{f}$:

$$a = 1 \tag{1}$$

$$\mathbf{f} = \mathbf{d_{remodeler}}. \tag{2}$$

Because of the underlying updates to $\mathbf{f}$ (see next subsection), this permanently writes with high signal strength the direction of travel of the first cell to pass through a particular ECM element.

Non-instantaneous signal writing

Anisotropy

Anisotropy is represented by a scalar ranging from 0 to 1, representing "complete lack of anisotropy" (or a disordered state) to "complete anisotropy" (a highly ordered state). The rate of change in anisotropy over time is given as:

$$\frac{da(\mathbf{x_i})}{dt} = r_a(1 - a(\mathbf{x_i})). \tag{3}$$

r_a is specified as:

$$r_a = r_{a0} s_{\text{cell}} \tag{4}$$

where r_{a0} is a base rate of change and s_{cell} is the migration speed of the cell changing the ECM anisotropy.

Orientation

Cells remodel the ECM by altering the fiber orientation $\mathbf{f}(\mathbf{x_i})$. We model that change as follows:

$$\frac{d\mathbf{f}(\mathbf{x_i})}{dt} = -r_f \left(\mathbf{f}(\mathbf{x_i}) - \frac{\mathbf{d_{remodeler}}}{||\mathbf{d_{remodeler}}||} \right) \tag{5}$$

with

$$r_f = r_{f0} s_{cell}(1 - a). \tag{6}$$

r_{f0} is the base rate of change and $\mathbf{d_{remodeler}}$ is the direction of the cell reorienting the fibers. $\boldsymbol{f}$ is normalized after each update. Note that when $a = 1$, orientation cannot change.

Density

Density ranges from 0 to 1, representing fluid filled tissue to very dense tissue completely filled with fibers, respectively. Cells change ECM density locally through the following relationship:

$$\frac{d\rho(\mathbf{x_i})}{dt} = r_{density}(\rho_{target} - \rho(\mathbf{x_i})) \tag{7}$$

where $r_{density}$ is the cell's characteristic rate of deposition/degradation of ECM and ρ_{target} is the cell's target for ECM density.

7.2 ECM influence on cell motility: Signal reading

Cell motion, in particular, cell speed and direction, can be altered via cell-ECM interactions. In a multicellular environment, this is the receiving step of communication enabling cells to communicate their paths to other cells. ECM element orientation and anisotropy are combined with a cell's preferred direction to produce the cell motility vector. Independently, cell speed is influenced by ECM density. We layout the orientation and anisotropy influences first, then the influence of ECM unit density. As with writing signals to the ECM, we define cells to be in and read whichever element their center coordinates are the closest to, as in [23].

ECM orientation and anisotropy

We developed a method to calculate $\mathbf{d_{actual}}$, a cell's actual motility direction, based on the cell's preferred direction $\mathbf{d_{preferred}}$, a cell specific ECM sensitivity s, and the local ECM's anisotropy and orientation. As illustrated in Figure 1d, we want to constrain cell motion to the sector spanning the ECM orientation ($\mathbf{f}$) and the cell's intended direction of travel ($\mathbf{d_{preferred}}$) in a way that does not bias direction of travel along the fibers. We use $\mathbf{f}$ and $\mathbf{d_{preferred}}$ to form an orthonormal basis set that spans the cell's potential directions (the sector produced by the angle θ in Figure 1d). We calculate $\mathbf{d_{actual}}$ by blending the

basis vectors using the cell's ECM sensitivity parameter s and local ECM element's anisotropy a as follows:

$$\mathbf{d_{actual}} = (1-\gamma)C_1\mathbf{d}_\perp + C_2\mathbf{f}, \tag{8}$$

where γ is the effective ECM influence parameter. This captures both cell sensitivity and ECM fiber alignment (signal strength):

$$\gamma = a \cdot s. \tag{9}$$

s and a are given as cell a parameter and from the local ECM element respectively. The other terms in Equation 8, the coefficients C_1 and C_2 and basis vector $\mathbf{d}_\perp$, are calculated by decomposing $\mathbf{d_{preferred}}$ and basic trigonometry.

We find $\mathbf{d}_\perp$, using the trigonometric relationship $\mathbf{A} \cdot \mathbf{B} = ||\mathbf{A}||||\mathbf{B}||\cos\,\theta$. Letting $\mathbf{f}$ and $\mathbf{d_{preferred}}$ be unit vectors and θ being the angle between them, the relationship simplifies to:

$$\mathbf{d_{preferred}} \cdot \mathbf{f} = \cos\,\theta. \tag{10}$$

Scaling $\mathbf{f}$ by that dot product, we get the component of $\mathbf{d_{motility}}$ that points along $\mathbf{f}$. Subtracting that result from $\mathbf{d_{motility}}$, we obtain a vector perpendicular to $\mathbf{f}$ as follows:

$$\mathbf{d}_\perp^{'} = \mathbf{d_{preferred}} - (\mathbf{d_{preferred}} \cdot \mathbf{f})\mathbf{f} \tag{11}$$

with normalization producing the unit vector $\mathbf{d}_\perp$ seen in Equation 8 and Figure 1d.

Note also that $\mathbf{d_{preferred}}$ can be decomposed as follows:

$$\mathbf{d_{preferred}} = C_1\mathbf{d}_\perp + C_2\mathbf{f} \tag{12}$$

with C_1 and C_2 the same as in Equation 8. They are determined via dot product and again, we take advantage of the terms being unit vectors:

$$\begin{aligned} \mathbf{d_{preferred}} \cdot \mathbf{d}_\perp &= (C_1\mathbf{d}_\perp + C_2\mathbf{f}) \cdot \mathbf{d}_\perp \\ &= C_1\mathbf{d}_\perp \cdot \mathbf{d}_\perp + C_2\mathbf{f} \cdot \mathbf{d}_\perp \\ &= C_1. \end{aligned} \tag{13}$$

Likewise, by dotting both sides of Equation 12 by $\mathbf{f}$, we obtain C_2 as follows:

$$\begin{aligned} \mathbf{d_{preferred}} \cdot \mathbf{f} &= (C_1\mathbf{d}_\perp + C_2\mathbf{f}) \cdot \mathbf{f} \\ &= C_1\mathbf{d}_\perp \cdot \mathbf{f} + C_2\mathbf{f} \cdot \mathbf{f} \\ &= C_2. \end{aligned} \tag{14}$$

With that, all required parts of Equation 8 are determined, letting $\mathbf{d_{preferred}}$ be calculated. Note that if the effective influence parameter γ is zero, Equation 8 becomes Equation 12. Likewise, when γ is one, its maximum value, $\mathbf{d_{preferred}}$ equals $\mathbf{f}$.

In the case that $\mathbf{d_{preferred}}$ is parallel to $\mathbf{f}$, $\mathbf{d}_\perp^{'}$ from Equation 11 is the zero vector. We assume the norm of the zero vector to be zero. With that set, the calculations will proceed as normal.

Note that there are two possibilities on how to interpret $\mathbf{d_{actual}}$:

A: The cell senses its environment, determines direction of travel along the fibers, and all cell effort goes into that motion.

B: The cell attempts to move both along the fibers and along its preferred direction, wasting effort in the process.

These two interpretations lead to either normalizing $\mathbf{d_{actual}}$ (Option **A**) or letting the cell direction vector lose magnitude by not normalizing $\mathbf{d_{actual}}$ (Option **B**). For the purposes of this work, we choose Option **B** and do not normalize $\mathbf{d_{actual}}$.

Constitutive relations to determine $\mathbf{d_{preferred}}$

To determine $\mathbf{d_{preferred}}$ in Equation 8, we extend the motility model of [23]'s motility model.

Chemotaxis based motility

To determine $\mathbf{d_{preferred}}$ for chemotactically motivated cells, we use the following equation from [23]:

$$\mathbf{d_{preferred}} = (1 - b) \cdot \mathbf{d_{random}} + b \cdot \mathbf{d_{chemotaxis}} \tag{15}$$

where $\mathbf{d_{random}}$ is a randomly generated unit vector, $\mathbf{d_{chemotaxis}}$ is a unit length microenvironment-derived direction, such as the gradient of a cell-required substrate, and the scalar b, running from 0 - 1, is the directional bias parameter that sets the balance between random (0) and completely biased cell motility (1). $\mathbf{d_{preferred}}$ is the cell selected motility direction and may be combined with local fiber orientation to produce the final cell motility direction.

ECM and chemotaxis based motility

To produce behaviors of both gradient and ECM following, we reformulated Equation 15 and replace the chemotactic bias with the local ECM anisotropy:

$$\mathbf{d_{motility}} = (1 - a) \cdot \mathbf{d_{random}} + a \cdot \mathbf{d_{chemotaxis}} \tag{16}$$

Here, a replaces the bias parameter in setting the random versus chemotactic behavior. When combined with the cell-ECM interactions, this model effectively enables a cell to only be chemotactic when in remodeled ECM.

History based motility

To generate a memory or hysteresis based motility, we alter the model in Equation 15 to include the anisotropy from the location of the most recent motility update, $a(\mathbf{x}_{\text{previous}})$, and a different bias parameter, b_{memory}, as follows:

$$\delta = a(\mathbf{x}_{\text{previous}}) \cdot b_{\text{memory}} \tag{17}$$

$$\mathbf{d_{preferred}} = (1 - \delta) \cdot \mathbf{d_{random}} + \delta \cdot \mathbf{d_{previous\ preferred}}. \tag{18}$$

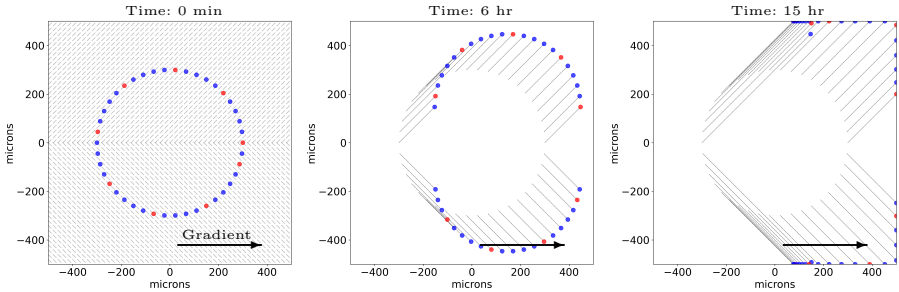

Supplementary Figure 1: **Highlight of individual aspects of the ECM-cell interactions: ECM orientation and cell chemotaxis** A combination of cues directing cell motility: ECM orientation (45° in the top of the domain and -45° in the bottom) and chemical gradient (to the right). The small black arrows trailing the cells show the positional history of each cell. The cell position is marked every 6 simulated minutes. Red and blue cells are identical; the coloring was added only for visual contrast.

δ incorporates both how sensitive the updated cell motility is to its most recent direction, $\mathbf{d}_{\textbf{previous preferred}}$ as well as how much fiber orientation there was to "remember" from the position of the most recent motility update.

ECM density

We use the following relationship to incorporate the influence of ECM density ρ on cell speed:

$$s_{\text{cell}} = \begin{cases} 0 & \text{if } \rho \leq \rho_l \\ S_{max} \frac{\rho - \rho_l}{\rho_{ideal} - \rho_l} & \text{if } \rho_l < \rho \leq \rho_{ideal} \\ S_{max} \frac{\rho - \rho_h}{\rho_{ideal} - \rho_h} & \text{if } \rho_{ideal} < \rho < \rho_h \\ 0 & \text{if } \rho \geq \rho_h \end{cases} \tag{19}$$

where ρ is the local ECM density, S_{max} is the maximum cell migration speed in $\frac{\mu m}{min}$, ρ_l is the ECM threshold density above which cells have non-zero speed, ρ_h is the ECM threshold density above which cells cannot move, and ρ_{ideal} is the ECM density of maximum speed.

This form simulates that in an actual fibrous environment a cell cannot move either when density is too low, due to a lack of fibers to grab onto for propulsion, or when density is too high, meaning the ECM is too dense for the cell to pass through. Other polynomials or curves derived from fitting to data could be used in place of this form. We choose it to be a minimum example of a tunable, potentially asymmetric curve with a local maximum.

7.3 Detailed parameter values

See Tables 2 to 5 for cell invasion parameters. Unless indicated otherwise, parameters are at default values for Physicell 1.4.1.

Parameter	Value	Range
Adhesion strength	5 μm/min	-
Repulsion strength	25.0 μm/min	-
Base cell speed	varies	0.25, 0.5, 1.0
Oxygen uptake	38 mmHg	-
Rate of proliferation	0 min^{-1}	-
Rate of death	0 min^{-1}	-
Chemotactic bias	Leaders - 0.95, followers - 0.05	-
Persistence time	10 min	-

Table 2: Cell-level parameters specific to the cell invasion model. Unless otherwise stated, parameters are at default values. In main results, adhesion strength was set to 10 μm/min unless otherwise stated. Likewise, cell speed was set to 0.25, 0.5, and 1.0 in main results and the bias varied with local anisotropy. In the SM, some results use a bias of 0.05.

Parameter	Value
Cell oxygen uptake	10 mmHg oxygen/min
Oxygen diffusivity	100,000 μm^2/min
Oxygen decay constant	0.1 mmHg oxygen/min
Boundary condition type	Dirichlet
Boundary condition value	38 mmHg oxygen
Computational mesh element size	20 by 20 by 20 μm^3

Table 3: Biotransport and chemical microenvironment parameters for cell invasion model.

Parameter	Value
Initial anisotropy	0
Initial density	0.5
Initial orientation	random
Fiber realignment rate (rate of change in anisotropy)	0.001 min^{-1}/0.004 min^{-1}
Fiber reorientation rate	1 min^{-1}/4 min^{-1}

Table 4: ECM initial conditions and remodeling parameters for all simulations.

7.4 Links to supplemental videos

7.4.1 Individual aspects of ECM-cell interactions videos

Figure 2a - Cell March

Figure 2b - Split ECM with chemotaxis

Figure 2c - Circular ECM with no gradient

Figure 2d - Circular ECM with chemical gradient.

Parameter	Value
Initial organoid radius	175 μm
Computational domain size	1600 μm by 1600 μm
Pre-mechanics microenvironment conditioning duration	10 min
Cell fraction of leaders	0.05 (main results)

Table 5: Tissue level parameters for cell invasion model. The parameter sweep (Section **??**) was done with a domain size of 1500 μm by 1500 μm. The results presented in the main body of the paper were done with a domain size of 1600 μm by 1600 μm.

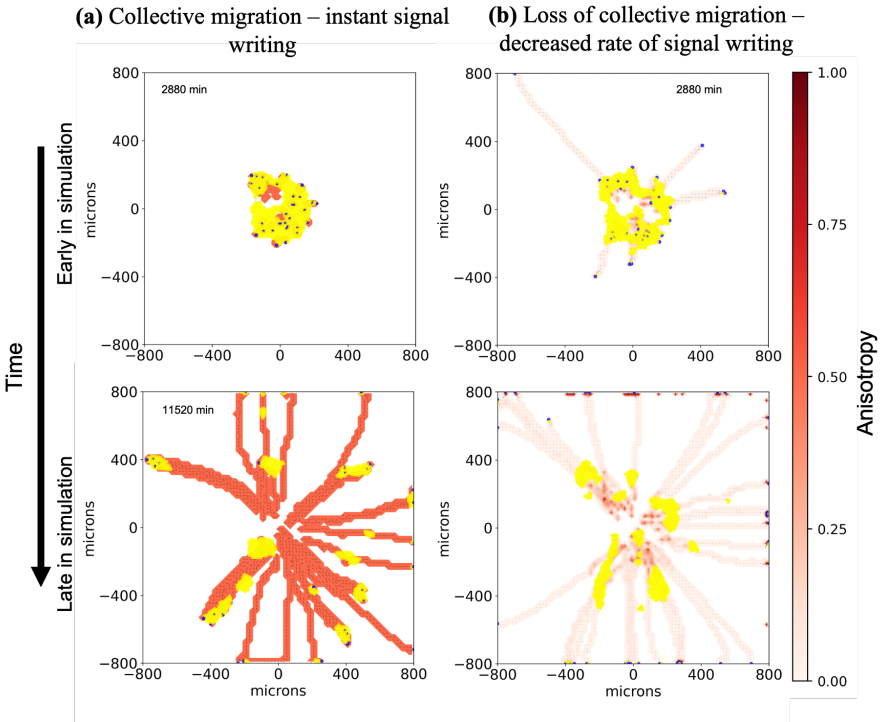

Supplementary Figure 2: **Collective migration requires sufficiently fast remodeling parameters** Figure 5a with instantaneous ECM remodeling contrasts with with **5**b which has relaxed the instantaneous signal writing and has remodeling rates slower than that in Figure 5b. Fiber realignment rate: 0.001 min^{-1}, fiber reorientation rate: 1 min^{-1}.

7.4.2 Collective migration is retained in the context of noisy communication videos

Instant signal writing

Non-instant signal writing

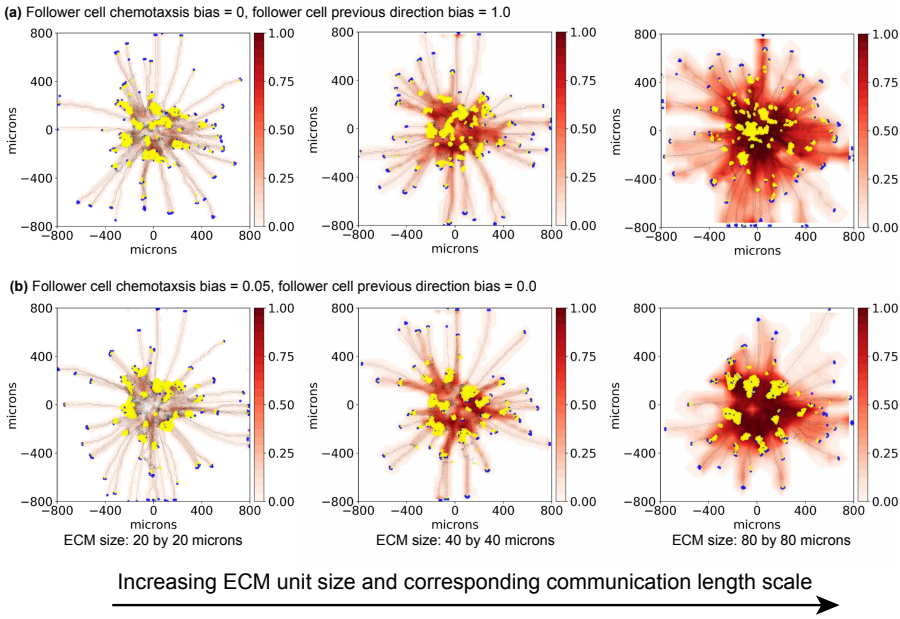

Supplementary Figure 3: **collective migration requires both increased length scale and direction** ECM unit size increases from left to right (20 by 20, 40 by 40, and 80 by 80 μm respectively). Row A shows results of memory-based follower motility updating (Equation 18) with b_{memory} set to 1.0. Row B shows results of giving followers with a mild chemotactic bias (b = 0.05) instead of a memory bias. All results produced with the same initial cell configuration and cell speed: 0.5 $\frac{\mu m}{min}$ and adhesion strength of 10 (μm/min). All results are shown at 48 hours of simulated time. Yellow circles: follower cells; Blue circles: leader cells. Red contours: ECM anisotropy values. See Supplemental Material Section 7.4.3 for full videos of each simulation, run out to 5 days of simulated time.

7.4.3 In depth exploration videos

Memory biased followers - 20 μm by 20 μm ECM

Memory biased followers - 40 μm by 40 μm ECM

Memory biased followers - 80 μm by 80 μm ECM

Chemotactic biased followers - 20 μm by 20 μm ECM

Chemotactic biased followers - 40 μm by 40 μm ECM

Chemotactic biased followers - 80 μm by 80 μm ECM